Nanoscale Swelling Heterogeneities in Type I Collagen Fibrils

Eike-Christian Spitzner,*,† Stephanie Röper,† Mario Zerson,† Anke Bernstein,‡ and Robert Magerle*,†

†Fakultät für Naturwissenschaften, Technische Universität Chemnitz, D-09107 Chemnitz, Germany and ‡Orthopädie und Traumatologie, Universitätsklinikum Freiburg, D-79095 Freiburg, Germany

ABSTRACT The distribution of water within the supramolecular structure of collagen fibrils is important for understanding their mechanical properties as well as the biomineralization processes in collagen-based tissues. We study the influence of water on the shape and the mechanical properties of reconstituted fibrils of type I collagen on the nanometer scale. Fibrils adsorbed on a silicon substrate were imaged with multiset point intermittent contact (MUSIC)-mode atomic force microscopy (AFM) in air at 28% relative humidity (RH) and in a hydrated state at 78% RH. Our data reveal the differences in the water uptake between the gap and overlap regions during swelling. This provides direct evidence for different amounts of bound and free water within the gap and overlap regions. In the dry state, the characteristic D-band pattern visible in AFM images is due to height corrugations along a fibril's axis. In the hydrated state, the fibril's surface is smooth and the D-band pattern reflects the different mechanical properties of the gap and overlap regions.

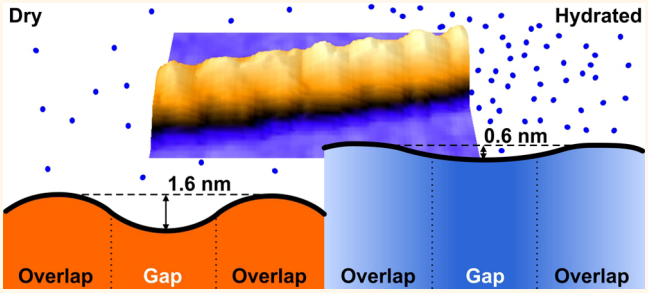

KEYWORDS: collagen · water · hydration · swelling · mechanical properties · dynamic atomic force microscopy

Collagens are a class of proteins that are a major constituent in the connective tissue of all vertebrates. Depending on their molecular conformation and supramolecular structure, collagen-based tissues, ranging from elastic skin, tendon, and ligament to stiff and tough materials like tooth or bone, display a wide range of mechanical properties.[1] Due to the abundance and versatile mechanical properties of collagen, a number of different research fields focus on the analysis and use of collagen, dealing with questions from a medical, materials science, chemistry, or physics perspective. Since the seminal work of Graßmann *et al.*,[2] collagen has been extensively studied on all length scales.[1] The hydrated-state studies of its structure and mechanical properties on the nano- and micrometer scale have only become possible since the introduction of methods[3−10] based on the atomic force microscope (AFM).[11] From previous work, it is clear that studying the distribution and structure of water within the collagen fibril is essential for understanding the relationship between the structure and the mechanical properties of collagen-based materials. Furthermore, gaining detailed insight into the nanoscale distribution of water within and between collagen fibrils is an important aspect in studies of biomineralization processes.[12−14]

A characteristic feature of the supramolecular structure of type I collagen fibrils is the so-called D-band pattern that originates in the staggering of the tropocollagen building blocks. Due to a periodic sequence of amino acids along the backbone of type I collagen molecules, a stripe pattern consisting of gap and overlap regions forms during fibrillogenesis.[1,15] This D-band pattern is observed in native collagen fibrils within different types of tissue (skin tendon, ligaments, cartilage, and bone) as well as in collagen fibrils reassembled *in vitro* in aqueous solutions containing dissolved tropocollagen. Recent works report on the statistical distribution of the D-band patterns in collagen-based tissues, possible changes in the D-band pattern, as well as changes in the fibrils' mechanical properties caused by diseases.[6,16,17]

AFM is widely used for imaging the nanoscale structure of collagen fibrils[3,18,19] and

* Address correspondence to ecs@music-mode.de, robert.magerle@physik.tu-chemnitz.de.

Received for review July 4, 2014 and accepted May 11, 2015.

Published online May 11, 2015
10.1021/nn503637q

for mapping their elastic modulus and viscoelastic response on the nanometer scale.[5,7−9,20−23] These measurements can be performed in the hydrated state, either in humid air or in aqueous buffer solutions.[5,7−9,18−24] In particular, the differences in the mechanical properties between fibrils in dry environment and in buffer solution have been investigated.[3,7−9] With AFM-based nanoindentation, Grant *et al.* measured the Young's modulus of type I collagen fibrils extracted from bovine Achilles tendon. They found that the Young's modulus decreases from 1.9 ± 0.5 GPa in the dry state to 1.2 ± 0.1 MPa in buffer solution.[8] The local mechanical properties of the D-band gap and overlap regions have been investigated in the dry state by Minary-Jolandan *et al.*[23] These fundamental studies of the shape, structure, viscoelastic properties, and deformation behavior of individual collagen fibrils form the basis for a detailed understanding of the nano- and micromechanics of structurally more complex collagen-based tissues.[4,6,10,16,17,25,26]

Here, we address the question of how water influences the shape and the mechanical properties of individual type I collagen fibrils on the nanometer scale. To this end, we perform a detailed analysis of the tip−sample interaction using multiset point intermittent contact (MUSIC)-mode AFM.[27] This imaging mode is based on the point-wise measurement of the amplitude and the phase of the AFM cantilever while the tip−sample distance is reduced. The resulting amplitude−phase distance (APD) curves allow for the reconstruction of a height image free from indentation artifacts[28−30] (corresponding to an amplitude set point of $A/A_0 = 1$) as well as height and phase images for a wide range of amplitude set points. The absence of a feedback loop as well as lateral forces further enhances the image quality. Additionally, the tip indentation into a compliant surface can be quantified,[31] and APD curves can be deconvoluted to discriminate between conservative and dissipative contributions to the tip−sample interaction.[32−34] Our MUSIC-mode AFM measurements reveal local differences in the swelling behavior of collagen fibrils, and we can quantify the local water uptake in the gap and overlap regions. These data corroborate recent modeling results on the distribution of water in collagen fibrils.[35]

RESULTS AND DISCUSSION

Collagen Fibril and Network Morphology. We study *in vitro* assembled type I collagen fibrils without telopeptides and without cross-links.[36] The fibrils are deposited on a polished silicon substrate and studied in air with controlled relative humidity. Figure 1 shows the IC-mode AFM height and phase images of collagen fibrils deposited on the substrate prior to and following the whole experiment. The morphology of the fibrils and the network is like that reported in other studies.[8,9,18,23,24,37,38] The fibrils differ in size, become thinner close to their ends, and are partly bent. Furthermore, the substrate is covered with a fine network that is also observed in other experiments[37,38] and which we call a collagen lawn.[39] It presumably

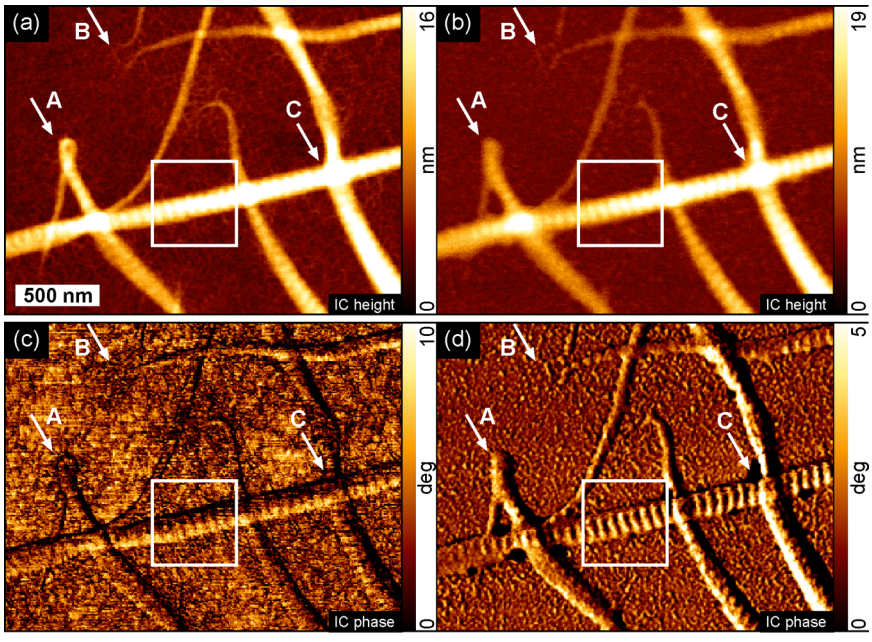

Figure 1. IC-mode AFM images of individual type I collagen fibrils deposited on a silicon surface measured at 28% RH. Height (a) and phase (c) images before the swelling procedure as well as height (b) and phase (d) images afterward. The white arrows point to structural changes that have occurred during the swelling procedure. The fast-scan axis is in the horizontal direction. Relative differences of height and phase values are shown. The display range was chosen to display structural details of both the fibrils and the collagen lawn.

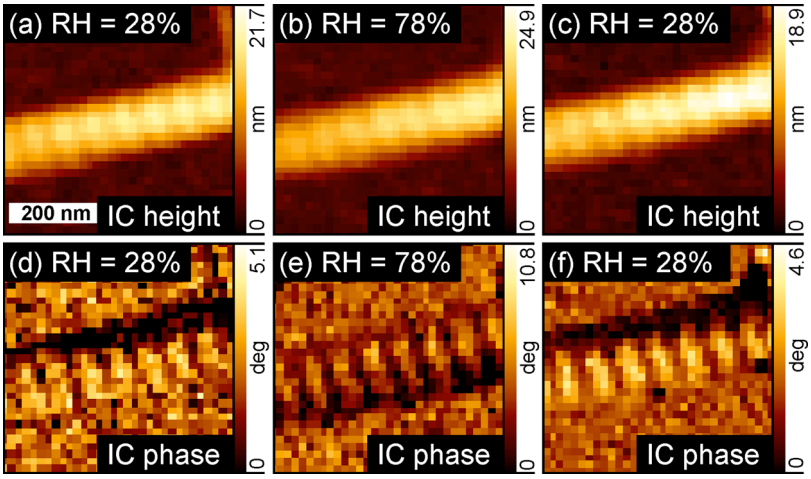

Figure 2. IC-mode AFM images of a fibril before swelling [height (a), phase (d)], after 20 h of swelling [height (b), phase (e)], and after drying [height (c), phase (f)]. The relative differences of height and phase values are shown. The RH is indicated in the panels.

consists of the residual constituents of the PureCol solution and, in particular, tropocollagen which did not self-assemble into larger fibrils.

In the IC-mode AFM phase image at the beginning of the experiment (Figure 1c), the collagen fibrils display phase values similar to those of the silicon substrate that is covered with the thin collagen lawn. If the mechanical properties of the collagen lawn are mainly dominated by the stiff substrate, the collagen fibrils can therefore be considered stiff. This is consistent with measurements of the elastic modulus of collagen fibrils in the dry state.[8,9] Figure 1b,d shows the sample surface again in the dry state but after the entire swelling and drying procedure. Although the overall structure looks the same, it differs in some details. For example, the loop on the left-hand side (marked with the arrow A) was previously open (Figure 1a,c) and has closed during the experiment (Figure 1b,d). The fibril's termini as well as the collagen lawn (marked with the arrows B) have changed their structure to that of small droplets. These small changes indicate that the tropocollagen molecules gain a certain mobility during swelling, leading to partial dewetting in the case of the lawn or a Plateau–Rayleigh instability in the case of the thin fibril's termini. The broadening is not an imaging artifact caused by a broadened AFM tip because we observe such shape changes also with fresh AFM tips. The white arrow C in Figure 1 marks one of the positions where dark spots are visible in the IC-mode phase image after the experiment. These dark spots appear along both sides of the fibrils, especially at the points of fibril intersection. We attribute the dark spots to an unknown minority component of the PureCol solution. Despite these small changes, the overall D-band structure of the large fibrils did not change during the swelling experiment. Before, during, and after swelling, we measured the mean D-band spacing over every fibril on $4 \times 4\ \mu m^2$ IC-mode AFM images. Within the accuracy of the measurement (<1 nm), no deviations from the value of 67 nm were found. This indicates that the collagen structure remained intact. We do not observe a decrease in the D-band spacing as reported after further dehydration by heating for several hours.[40]

For the detailed discussion of the contrast in the IC-mode AFM images, we focus on a section of the straight fibril (marked with a white rectangle in Figure 1) that remained stable during the entire experiment. Figure 2 shows the IC-mode height and phase images at 28% RH (Figure 2a,d), after swelling for 20 h at 78% RH (Figure 2b,e), and finally dried again at 28% RH (Figure 2c,f). In all three cases, the same section of seven D-periods of the same fibril is shown. The D-period is always visible in the height as well as in the phase images. The conventional interpretation of these images leads to the conclusion that, whether the fibril is hydrated or not, the fibril's surface exhibits a similar height undulation with a D-periodicity of 67 nm. Furthermore, the mechanical properties, as reflected in the IC-mode phase images, also suggest a similar situation in the dry state and the hydrated state, with stiffer regions at the D-band overlap (higher phase values) and softer gap regions (lower phase values). We will show that this interpretation is not correct because the IC-mode images are subject to several imaging artifacts.

Swelling Behavior of Collagen Fibrils. Figure 3a–c shows the MUSIC-mode height images z_0 for $A/A_0 = 1.00$ of the same spot shown in Figure 2. In the dry state before (a) and after swelling (c), the height undulations with the D-periodicity are clearly visible as in the IC-mode height images. However, in the hydrated state (b), hardly any D-band structure is visible, pointing toward a different shape of the fibril's surface in the hydrated state. In the MUSIC-mode height images, we measured the height and width of this section of the fibril (Table 1).

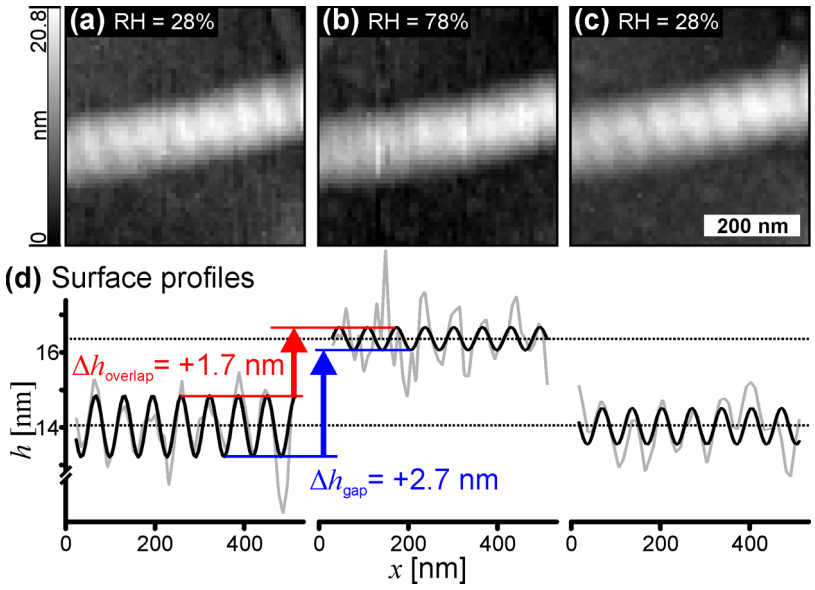

Figure 3. MUSIC-mode images of the unperturbed height z_0 before (a), during (b), and after (c) swelling. (d) Mean of four adjacent profiles along the fibril's main axis (gray) and a sinusoidal fit (black). The dotted lines are the averages along the fibril's axis (see Table 1).

TABLE 1. Mean Height and Full Width at Half-Maximum of the Fibril Shown in Figure 3,[a]

	height (nm)	width (nm)	Δh_{PP} (nm)
28% RH (before)	14.1	114	1.6 ± 0.1
78% RH	16.3	117	0.6 ± 0.2
28% RH (after)	14.1	114	1.0 ± 0.1

[a] The values are calculated from 12 cross sections perpendicular to the fibril's main axes. Right column: Peak-to-peak amplitude, Δh_{PP}, of the sinusoidal fit shown in Figure 3d.

The mean height increases by 2.2 nm during swelling, and the fibril broadens by 3 nm (full width at half-maximum). Note that the tip convolution leads to an increase in the apparent width, an increase that is independent of the degree of swelling. Since the measured mean changes in height and width during swelling are fully reversible, the water uptake is reversible. Within the area shown in Figure 1, we also measured the height of other fibrils in the dry (h_D) and the hydrated state (h_H). In all cases, we observe a 15% increase in height (Figure 4), which we interpret as swelling of the entire fibril through water uptake. The 15% increase in height corresponds to the increase of the tropocollagen crystal lattice constant as reported by Lees,[41] who investigated the lattice constant of different types of collagen fibrils as a function of their water content. For type I collagen extracted from rat tail tendon, a change in the water content from 0.3 $g_{(H_2O)}/g_{(collagen)}$ to 0.8 $g_{(H_2O)}/g_{(collagen)}$ leads to an increase in the lattice constant of 15%.

An additional contribution to the increase of the fibrils' height with increasing relative humidity could be the adsorption of water on the surface of the specimen and on the AFM tip. These layers of adsorbed

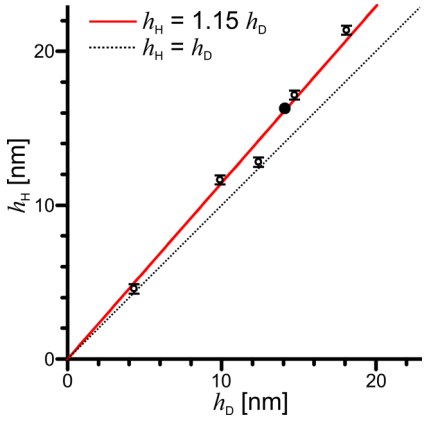

Figure 4. Height h_H of fibrils in the hydrated state (78% RH) plotted as a function of their initial height h_D in the dry state (28% RH). Data from IC-mode (○) and MUSIC-mode (●) AFM height images are shown. The red line is a linear fit to the data, and the dotted line is the reference to $h_H = h_D$.

water play an important role in the tip−sample interaction, and we will discuss it below. Since a fibril's height is measured relative to the surface of the collagen lawn, only the difference in the increase of the water layer on the collagen fibril compared to that on the collagen lawn can affect the measured height of the fibril. Moreover, the thickness of the layer of adsorbed water should not depend on the total thickness of the fibril and therefore cause a constant offset Δh when plotting h_H over h_D (Figure 4). Since we do not observe such an offset, we conclude that the adsorbed water does not affect the measurements of the fibril's height.

In addition to the overall swelling of the whole fibril, the mean height profile along the fibril's main axis shows that the height contrast between the gap and

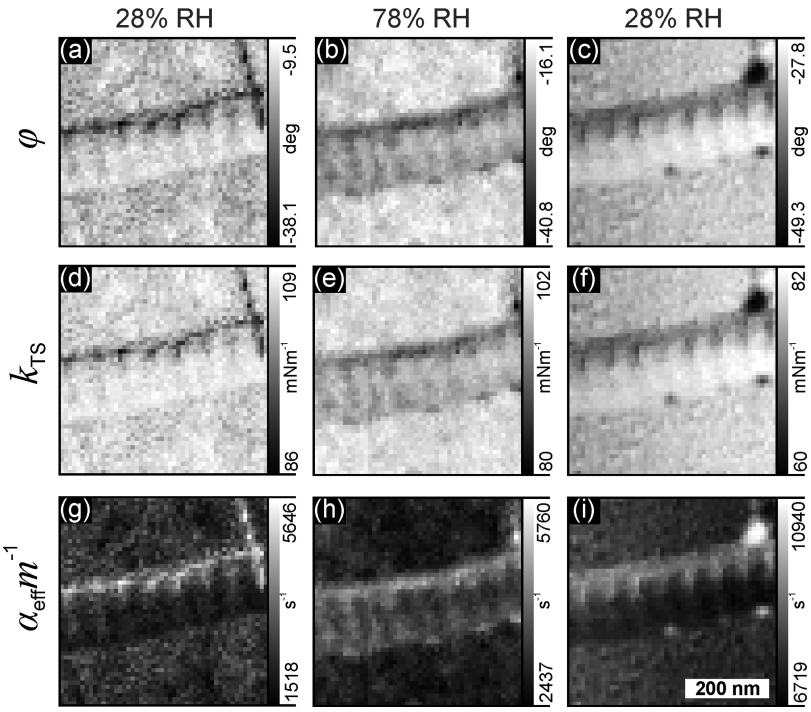

Figure 5. (a–c) MUSIC-mode AFM phase images of the fibril shown in Figure 3 as well as the conservative (d–f) and the dissipative (g–i) contributions to the tip–sample interaction. For all images, $A/A_0 = 0.50$.

overlap regions along the D-band structure is smaller in the hydrated state (Figure 3d). To quantify this effect, a sinusoidal curve with a fixed D-period of 67 nm was fitted to the data. The peak-to-peak amplitude, Δh_{PP}, of the height corrugation is 1.6 nm in the dry state; it decreases to 0.6 nm in the hydrated state, and it increases to 1 nm when the fibril is dried again (Table 1). This reveals only a tiny height contrast of the gap–overlap structure along the hydrated fibril, as seen in the MUSIC-mode height image (Figure 3b). The data shown in Figure 3 and Table 1 reveal the differences in the water uptake between the gap region and the overlap region during swelling. In the gap region, the fibril's height increases by $\Delta h_{gap} = 2.7$ nm, whereas in the overlap region, it increases by $\Delta h_{overlap} = 1.7$ nm (Figure 3d). This provides direct evidence for different amounts of bound and free water within the gap and overlap regions. This is a central result which we will discuss in detail below.

Conservative and Dissipative Tip–Sample Interactions. The conventional IC-mode phase images (Figure 2d–f) show the same pattern in all three cases (before, during, and after swelling), with an increased gap–overlap contrast in the hydrated state. The MUSIC-mode results at an amplitude set point of $A/A_0 = 0.50$ are shown in Figure 5, where the phase images (φ) as well as the conservative (k_{TS}) and the dissipative (α_{eff}/m) contributions to the tip–sample interaction are shown. In the dry state, the fibril exhibits little contrast in the phase image (Figure 5a). Only a region of lower phase values is discernible at the top side of the fibril at the three-phase contact line between the fibril, the substrate, and the air. Also, the D-band structure is only slightly visible. The same applies for the image of k_{TS} (Figure 5d) and, with inverted contrast, the α_{eff}/m image (Figure 5g). These results indicate a very small mechanical contrast between the gap and overlap regions in the dry state.

In the hydrated state at 78% RH, the contrast in the MUSIC-mode phase image increases. This is in line with the contrast in conventional IC-mode AFM phase images, but the fibril's structure looks different in the MUSIC-mode images at 78% RH (Figure 5b,e,h). Here, there are darker areas along both sides of the fibril as well as in the gap of the D-period. This ladder-like structure is best seen in the image of α_{eff}/m. This suggests that dissipative tip–sample interactions are the main origin of the phase contrast.

After the fibril has been dried again (Figure 5c,f,i), the MUSIC-mode images show the same structure as in the initial dry state with only tiny differences in the mechanical properties of the gap and overlap regions. In addition, the images show that the fibril was not altered by the MUSIC-mode measurements. In particular, the deformation of the surface due to the indentation of the tip into the surface is fully reversible. In the dry state, a softer region is visible at the top side of the fibril. This effect could be explained by an asymmetric tip shape. In the hydrated state, however, both sides of the fibril exhibit similar mechanical properties, comparable to the softer gap regions. Together with the gap–overlap variations, this results in the previously described ladder-like structure (Figure 5b,e,h). Since both sides of the fibril show softer

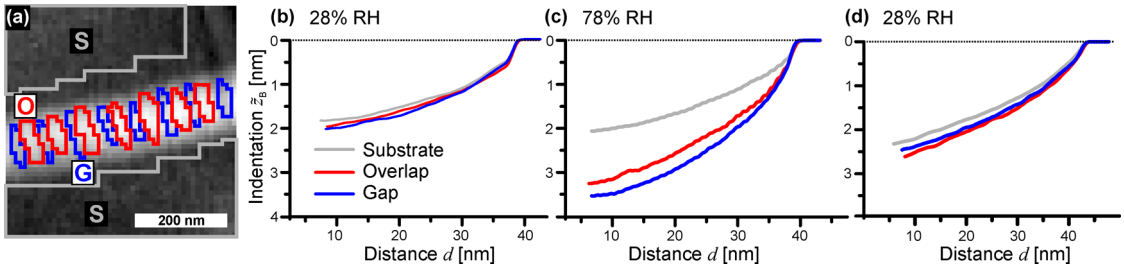

Figure 6. (a) MUSIC-mode height image z_0 of the fibril in the dry state with the regions on the substrate (S), overlap (O), and gap (G) which were selected to calculate the mean indentation. (b–d) Mean indentation of the tip into the sample surface ($\tilde{z}_B$). (b) On the fibril at 28% RH, (c) hydrated at 78% RH, and (d) dried again at 28% RH. The averages of the curves from the regions marked in (a) are shown. Substrate: (b) 1293, (c) 1287, and (d) 746 positions. Gap region: (b) 145, (c) 280, and (d) 182 positions. Overlap region: (b) 194, (c) 154, and (d) 240 positions.

material, this cannot be explained by the tip shape because neither the tip nor the sample orientation was changed compared to the experiments in the dry state. Hence, we suppose that the softer edges of the fibril in the hydrated state are not an imaging artifact but mechanical properties that correlate with the local height of the fibril. Within the imaged area, small fibrils with a height smaller than ≈3 nm broaden (spread) during swelling (Figure 1, arrows A and B). Therefore, we assume that the edges of the fibril become softer in the hydrated state because of their small thickness.

Tip Indentation. The MUSIC-mode data provide the unperturbed height z_0 as well as the tip indentation $\tilde{z}_B$, which gives further insight into the local mechanical properties of the fibril's surface. The tip indentation is plotted in Figure 6 as a function of the tip–sample distance.

In the dry state, the tip indentation $\tilde{z}_B$ into the fibril is ≈0.2 nm larger than that on the substrate, but hardly any differences are apparent between the gap and overlap regions. This is in line with the previously discussed homogeneous mechanical properties of the fibril in the dry state. In the hydrated state, the average indentation $\tilde{z}_B$ into the fibril's surface increases by up to 1.5 nm and is 0.3 nm larger in the gap regions than in the overlap regions (Figure 6c). The value of the indentation $\tilde{z}_B$ further indicates that the fibril behaves as a solid material in the hydrated state because the maximal tip indentation is only 3.5 nm. On compliant (soft) surfaces, like amorphous polymers above the glass transition temperature, the tip indentation can reach up to 20 nm for the given tip oscillation parameters.[30,42,43] On the substrate, which is covered with a collagen lawn, the tip indents up to 2 nm into the surface in the dry as well as in the hydrated state, which corresponds well to the laterally averaged thickness of the adsorbed collagen layer.[39] Our tip indentation data show that the thickness of the collagen lawn does not increase upon hydration.

Local Mechanical Properties. With AFM nanoindentation experiments, Minary-Jolandan *et al.*[23] investigated the Young's modulus of type I collagen fibrils at 12% RH and measured 1.2 GPa in the gap region and 2.2 GPa in the overlap region. Such large values are typical for solid, glassy polymers.[44] This explains the weak contrast between the gap and overlap regions in the MUSIC-mode images of the phase as well as in the conservative k_{TS} and dissipative α_{eff}/m contributions to the tip–sample interaction (Figure 5). The large contrast in the conventional IC-mode phase images in the dry state is astonishing given the values of the Young's modulus. We therefore conclude that this large phase contrast is mainly a result of feedback loop artifacts, which are also the reason for the structure that is visible in the conventional IC-mode AFM amplitude images (cf. Figure 1a in ref 17). Feedback loop artifacts are probably also the reason why the D-period of the fibrils oriented along the fast-scan axis (horizontal direction in Figure 1) is better visible in the conventional IC-mode phase images than the D-period of fibrils oriented perpendicular to the fast-scan axis (vertical direction in Figure 1).

The MUSIC-mode height image in the hydrated state indicates local differences in the swelling behavior. The gap regions gain more volume compared to the overlap regions, which causes the height contrast between the gap and overlap regions to decrease. This renders the D-band structure almost invisible in the MUSIC-mode height image for $A/A_0 = 1$, which corresponds to the shape of the unperturbed surface. This is the case for both the image of z_0 (Figure 3) and the image of z_B (not shown). Furthermore, these differences in the uptake of water lead to distinct differences in the local mechanical properties. The gap region, which swells more compared to the overlap region, becomes significantly softer than the overlap region. This explains why the tip indentation in the gap region is half a nanometer larger than that in the overlap region. This difference results in an indentation artifact in the conventional IC-mode height image, which causes height undulations in the hydrated state similar to those in the dry state.

After the fibril has been dried again, the height undulation and the tip indentation reach values similar to those in the dry state before swelling. We attribute the small difference to an incompletely dried

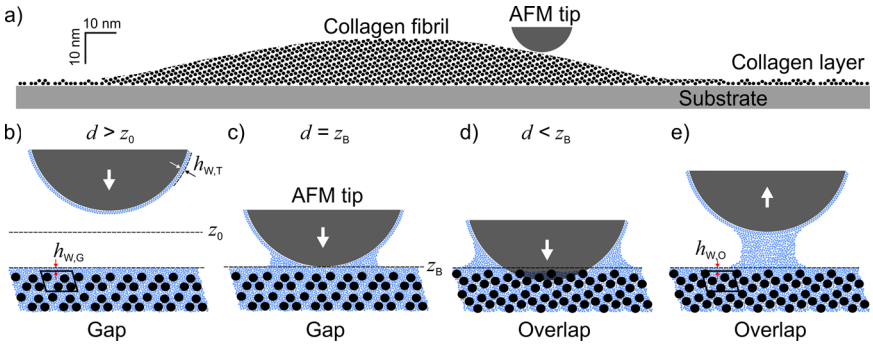

Figure 7. (a) Cross section of the collagen fibril (perpendicular to its main axis) studied with MUSIC-mode AFM (Figure 3). (b–e) Model of the tip–sample interaction and the fibril's molecular structure according to Streeter *et al.*[35] Black and blue dots correspond to tropocollagen and water molecules, respectively. The AFM tip is shown (from left to right) before any interaction between the tip and the sample occurs (b), at the position z_B where attractive and repulsive interactions balance each other (c), with an indentation of 1.5 nm into the fibril's surface (d), and when it retracts and a water meniscus forms (e).

fibril because the sample was kept for 1 day at 28% RH before imaging it for the first time in the dry state. After 20 h of swelling, the relative humidity decreased exponentially within 15 h. Values below 30% RH were reached just a few hours before imaging the fibril in the dry state for the second time (see Materials and Methods section). Therefore, it is likely that the fibril's water content was slightly higher at the end of the experiment than at the beginning.

Model of the Tip–Sample Interaction. The distribution of water within the tip–sample contact region is essential for understanding the capillary forces between the AFM tip and the specimen. Water is known to form a wetting layer on hydrophilic surfaces, such as the SiO_x-covered surface of the AFM tip, which is made of silicon. Ellipsometry data show that, on a flat silicon oxide surface, the water wetting layer has a thickness of 0.1 nm at 28% RH and 0.3 nm at 78% RH.[45] With infrared spectroscopy, Asay *et al.* found a thicker and a partly ice-like layer of water.[46] With contact-mode AFM, they studied the effects of adsorbed water on the adhesion force between a silicon AFM tip and a silicon oxide surface.[47] Zitzler *et al.* studied capillary forces in tapping-mode AFM and have shown that the detailed shape of APD curves can be quantitatively explained "in a model based on the intermittent formation of a capillary neck between tip and sample close to the lower turning point of the cantilever oscillation".[48] "When tip and sample are in contact the water in the overlapping region is displaced and accumulated at the edge of the contact area. This amount of water [...] is assumed to form a meniscus when the tip is retracted".[48] The schematic shown in Figure 7b–d is based on this model.

Figure 7 is a graphical compilation of the available data on the fibril's shape and molecular structure as well as the structure of the tip–sample contact region. The fibril's cross section (Figure 7a) is the measured height profile of the fibril shown in Figure 3. The distance and pattern of dark dots corresponds to the position of tropocollagens within the crystal lattice of type I collagen fibrils.[35] The thickness of the collagen lawn is 2 nm.[39] The width of the attractive regime, $z_0 - z_B$, is 4 nm in our experiment (see Materials and Methods section). The fibril's cross section shows that the fibril adsorbs flat onto the substrate, which is also observed in other experiments.[37,38] This flat shape is in stark contrast to the presumably round shape formed during the self-assembly in buffer solution.[1] The fibril's width is too large to be affected by convolution with the tip shape. The fibril's height (Table 1) corresponds to about 12 layers of tropocollagen. The tropocollagen layer that is adsorbed at the substrate (the collagen lawn) has a thickness of about one to two tropocollagen layers. The collagen fibril is much wider than the typical diameter of the AFM tip. Therefore, the geometry of the tip–sample contact can be approximated as a sphere above a planar surface (Figure 7b–d). We assume a tip radius $r = 10$ nm and for the thickness of the water layer on the SiO_2-covered AFM tip, $h_{W,T}$, a value of 0.1 nm at 28% RH and 0.3 nm at 78% RH as reported in ref 45. These values also correspond to the thickness of the layer of liquid water reported in ref 46. Similar thicknesses have been measured for the water layer on mica, which is also a hydrophilic surface.[45] Since collagen is hydrophilic, we assume that a thin water layer is also present on the fibril's surface as well as on the collagen lawn that covers the substrate. For reasons of simplicity, we assume a thickness of these water layers similar to that on silicon oxide; however, the following arguments are compatible with thicker layers of water on the collagen fibril and on the collagen lawn.

When the oscillating AFM tip approaches the surface, two characteristic positions can be distinguished. The position, when the inflection point of the oscillating tip is at the onset of attractive forces, defines the unperturbed sample surface z_0, according to ref 30. This surface lies above the alternative definition of the sample surface, z_B, which we define as the position where the balance of attractive and repulsive forces is observed in the phase–distance curves

(see Materials and Methods section). In analogy to ref 48, we assume that, at this position, the tip has partially displaced water from the tip−sample contact region and started to push against the tropocollagen molecules (Figure 7c). Finally, as the tip indents into the fibril's surface, tropocollagen molecules are displaced from their natural lattice position (Figure 7d). At 78% RH, we observe a maximal indentation $\tilde{z}_B$ of 3.5 nm in the gap regions and 3.2 nm in the overlap regions (Figure 6). This corresponds to a thickness of two layers of tropocollagen molecules. At the ridge of the fibril, this is not a large deformation for a 16 nm thick fibril. The difference $z_0 - z_B$ is the width w of the attractive regime. Two factors contribute to it: (a) the formation of a water meniscus and (b) attractive van der Waals forces between the tip and the specimen.[48] The width of the attractive regime increases with increasing tip radius.[49] Another characteristic quantity is the length of the water meniscus that forms when the tip retracts from the contact region (Figure 7e). It can be defined in static (contact-mode) force−distance curves as the snap-off position when the tip retracts from the surface.[48] For tips with 10 nm radius, both the width of the attractive regime and the length of the water meniscus are several nanometers large. We note that the difference, $w = z_0 - z_B$, is the same in the dry state (28% RH) and the hydrated state (78% RH) on the collagen fibril as well as the thin collagen lawn. Therefore, the measurement of the fibril's height does not depend on which definition of the sample surface is used.

Water in Type I Collagen Fibrils. An explanation for the different swelling behavior of the gap and the overlap regions can be found in the simulation results of Streeter *et al.*[35] With molecular dynamics simulations, they modeled the molecular structure of type I collagen fibrils in the presence of water and chloride ions. They found that two species of water are present within the fibril. First, there is free water filling the space between the individual tropocollagens, and second, there are water molecules which serve as bridges for hydrogen bonds between tropocollagens and are therefore more tightly bound. In the gap region, the density of interprotein water bridges is found to be 34% lower compared to the overlap region.[35] When the fibrils, which self-assembled in buffer solution, are deposited onto the substrate and dry, water evaporates and the inter-tropocollagen distance (the lattice constant) decreases.[41] Moreover, the gap loses more water since its water content is higher due to the 20% lower tropocollagen density and due to the smaller amount of water bound in interprotein water bridges.[35] The local differences in the amount of free water lead to local differences in the shrinking and, in turn, to the shape undulations visible in AFM height images of dry collagen fibrils. During swelling at elevated relative humidity, the gap regions absorb more water and become more compliant (softer) than the overlap regions. Our observation that the height corrugations are diminished in the hydrated state is consistent with the driving force of the surface tension, which also minimizes the surface undulations.

Figure 7d shows the AFM tip at its inflection point, with a 1.5 nm tip indentation with respect to the surface z_B. The crystal lattice of tropocollagen (black dots) must deform to allow for such an indentation. This deformation is elastic because the fibril's shape is not altered by the MUSIC-mode AFM measurements. In the dry state, we observe no distinct contrast in the images of k_{TS}, the conservative contribution to the tip−sample interaction (Figure 5d,f), and the average indentation $\tilde{z}_B$ (Figure 6b,d), despite the 20% difference in the tropocollagen density between the gap and overlap regions.[35] One reason for this could be the greater shrinkage of the crystal lattice in the gap region due to the greater loss of water during drying. This shrinkage of the lattice constant of the gap regions not only causes the height undulations, which are visible in the AFM height images of dry fibrils, but also reduces the tropocollagen density difference between the gap and overlap regions. This effect could explain the smaller contrast in the images of the effective damping parameter in the dry state (Figure 5g,i).

In the hydrated state, the fibril's mechanical properties change. Figure 7b,c shows the gap region in the hydrated state with the unperturbed tropocollagen lattice (similar to the situation after fibrillogenesis in aqueous solution), for which we would expect no height undulations. The tropocollagen density difference of 20% between gap and overlap regions leads to an enhanced contrast in the image of the conservative contribution to the tip−sample interaction, k_{TS} (Figure 5e). However, the dissipative interactions are the main contribution to the contrast of the MUSIC-mode phase images (Figure 5b). In the gap regions, more free water is present in the larger interprotein space and the free water is more mobile; therefore, the tropocollagen crystal lattice can be more easily deformed by the AFM tip than in the overlap regions. The tip indentation causes a temporary redistribution of the free water within the deformed contact zone, which is a dissipative process. At low amplitude set points, A/A_0, when the tip indentation is large, this process becomes more important and differences between the gap and overlap regions cause an increasing contrast in the images of the dissipative contribution to the tip−sample interaction, α_{eff}/m (Figure 5h).

CONCLUSIONS

With MUSIC-mode AFM, we investigated the tip−sample interaction with a type I collagen fibril in the dry and the hydrated state. Our results show how the distribution of water within the fibril controls their swelling behavior, shape, and mechanical properties on the nanometer scale.

The average degree of swelling corresponds to the known dependence of the collagen lattice constant on the water content.[41] We observe differences in the swelling of the gap and the overlap regions, which we explain by the different amounts of free water in the interprotein space. This corroborates recent computer simulation results on the structure and molecular dynamics of water in collagen fibrils.[35]

In the dry state, the D-band structure is a height undulation along the fibril's main axis. The height differences between gap and overlap regions are due to differences in shrinking that reflect different amounts of free water in the gap and overlap regions. Both types of regions show the same mechanical properties in the tip indentation as well as in the conservative and dissipative contribution to the tip–sample interaction.

In the hydrated state, the fibril surface is smooth and the D-band structure is due to the different mechanical properties of the gap and the overlap regions. The hydrated collagen fibril still behaves as an elastic solid: in the overlap and the gap regions, the maximal tip indentation is only 3.2 and 3.5 nm, respectively. The difference in tip indentation is accompanied by different viscoelastic properties of the gap and overlap regions. The largest difference (contrast) is observed in the dissipative contribution to the tip–sample interaction, which we attribute to the differences in the amount and structure of water in the interprotein space.

From a more general perspective, MUSIC-mode AFM imaging under conditions of controlled humidity and temperature allows the study of nanoscale swelling phenomena with unprecedented detail. This is of particular interest for biomimetic interfaces and hydrogels. We expect that this approach will be beneficial for studies of soft, hydrated surfaces of biological and bioinspired materials as well as polymer surfaces of technological importance.

MATERIALS AND METHODS

Sample Preparation. We investigated purified type I collagen isolated from bovine hide (PureCol from INAMED, Fremont, USA). It was purchased as an aqueous solution (3 mg/mL) with a pH of 2. The collagen extraction procedure is described in ref 36. A drop of buffer solution (30 μL, L-glycin/KCl, pH 9.2) was deposited on a freshly cleaved mica substrate, and 2 μL of the collagen solution was injected. After 60 min adsorption time on mica, 60 μL of buffer solution was injected and individual collagen fibrils were picked up with a micropipette, deposited onto a silicon surface, and spread with the micropipette. After drying the sample in air, we flushed the sample surface with distilled water to remove residual buffer crystals. Prior to fibril deposition, the 1 $\times$ 1 cm^2 large silicon substrate with a native SiO_x layer was cleaned for 20 min in a 1:1 solution of acetone/toluene. After the substrate was removed from the cleaning solution, it was mounted on a heating plate (150 °C), and the residual contamination was subsequently removed with a jet of carbon dioxide.[50] The entire sample preparation procedure resulted in a network of isolated collagen fibrils deposited on a silicon substrate, similar to that in previous works.[8,9,18,23,24,37,38]

Humidity Control. For AFM measurements under controlled humidity, we used a custom-built setup consisting of a sealing ring and a washing bottle filled with water, similar to commercially available systems.[51] The humidity was regulated *via* the air flow, which was adjusted with a pressure-regulating valve. The resulting humidity and the temperature were recorded with an SHT75 sensor (Sensirion AG, Staefa, Switzerland) and are shown in Figure 8. We imaged individual collagen fibrils with AFM in conventional IC mode[52] as well as in MUSIC mode,[27] first at 28% RH after swelling for 20 h at 78% RH and imaging at 78% RH and 15 h after we switched off the air flow that provided the elevated humidity (imaging at 28% RH).

AFM Imaging. All of the AFM measurements were performed using a Nanowizard I instrument (JPK Instruments AG, Berlin, Germany). At ambient conditions (28% RH), the silicon AFM cantilever (Pointprobe NCH, NanoWorld AG, Neuchâtel, Switzerland) had a resonance frequency ω_0 = 280.526 kHz, a quality factor Q = 449, and a spring constant k = 21.1 N/m (determined as in ref 53). The typical tip radius was <8 nm, as specified by the manufacturer. At 78% RH, the cantilever parameters changed to ω_0 = 280.510 kHz, Q = 454, and k = 21.2 N/m. After the relative humidity decreased to 28%, the values were ω_0 = 280.362 kHz, Q = 242, and k = 11.7 N/m.

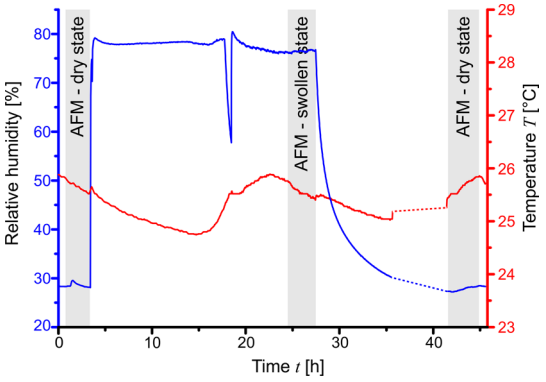

Figure 8. Relative humidity (blue) and temperature (red) in the AFM liquid cell during the experiment. The gray stripes mark the time where the AFM measurements took place.

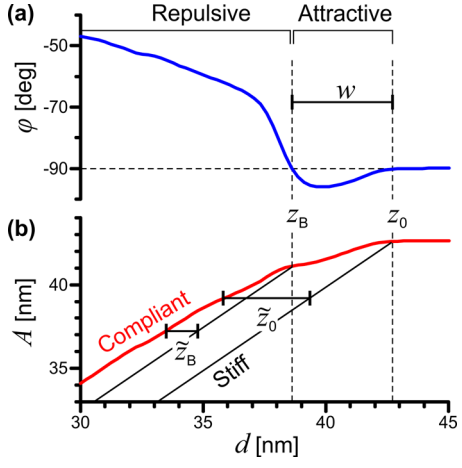

Figure 9. (a) Phase φ and (b) amplitude A measured on a collagen fibril (28% RH) as a function of the tip–sample distance d (approach curves). The thin solid lines indicate the amplitude on an stiff reference surface.

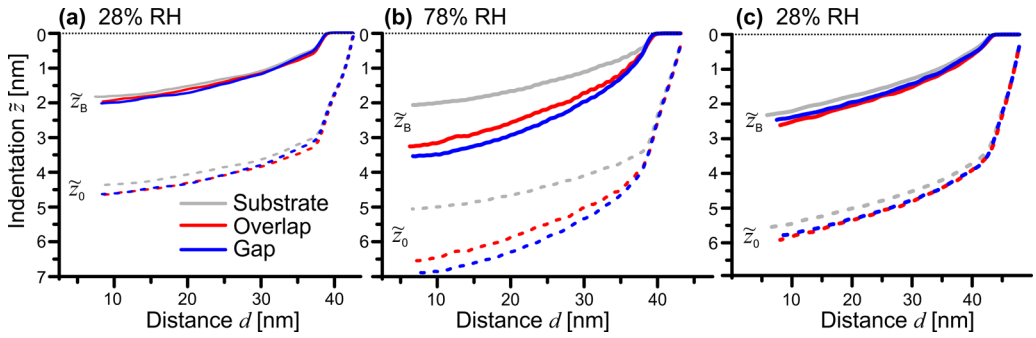

Figure 10. Mean indentation of the AFM tip into the sample surface as a function of the tip−sample distance at 28% RH (a), in the hydrated state at 78% RH (b), and dried again at 28% RH (c). Two definitions of the unperturbed sample surface were used: the onset of attractive forces z_0 (dashed lines) and the balance of attractive and repulsive forces z_B (solid lines).

The MUSIC-mode protocol is described elsewhere.[27] To reconstruct the MUSIC-mode AFM images, arrays of 50 × 50 amplitude−phase distance curves were measured in each case. The APD curves were separated by 10 nm, resulting in images that were 500 × 500 nm^2 large. Small positional variations of the imaged areas in the dry and the hydrated states are possible. Nonetheless, within one series of MUSIC-mode images, every map shows exactly the same spot. The APD curves were obtained at the free resonance frequency of the cantilever. The free amplitude A_0 was measured to be 43 nm, and the minimum amplitude A_{min} was set to 10 nm. Prior to and after the MUSIC-mode measurements, the sample surface was imaged with conventional IC-mode AFM to provide an overview and to determine the thermal drift in the $x-y$ direction that took place during the APD curve recording. It turned out that the thermal drift was negligible, and therefore, no registration of the MUSIC-mode images was necessary.

Data Analysis. The APD curves were analyzed as described in refs 30, 31, and 34. Briefly, the influence of the tip−sample interaction on the forced oscillation of the AFM cantilever is modeled using first-order perturbation theory.[34] Conservative and dissipative contributions to the total tip−sample interaction force are expressed by an additional tip−sample spring constant k_{TS} and the effective damping parameter α_{eff}/m. The former is given by

$$k_{TS} = k_{eff} - k = m\left(\omega^2 + \cos(\varphi)\,\frac{F_0/m}{A}\right) - k \qquad (1)$$

where $m = k/\omega_0^2$ is the vibrating mass and k_{eff} is the total effective spring constant. The effective damping parameter is

$$\alpha_{eff}/m = \frac{-\sin(\varphi)}{\omega}\,\frac{F_0/m}{A} \qquad (2)$$

The quantity F_0/m, where F_0 represents the amplitude of the excitation force, is obtained by fitting the cantilever resonance curve.[34]

MUSIC-mode AFM images of the height, phase, k_{TS}, and α_{eff}/m were reconstructed for amplitude set points ranging from $A/A_0 = 1$ to $A/A_0 = 0.25$. All height images were first-order flattened, whereas the other maps were not postprocessed. Image analysis was conducted using the ImageJ software.[54]

Tip Indentation. For a given amplitude $A < A_0$, the tip indentation into a compliant surface is the additional distance Δd that the tip has to approach the surface in order to reach the same damped amplitude A as on a stiff reference surface that does not allow for any indentation.[31] The tip indentation depends on the definition of the unperturbed surface (Figure 9). The point of first contact (z_0) is often defined by the first appearance of attractive interaction as the tip approachs.[30,31,42,43] In many cases, this choice leads to reliable results. However, in the case of collagen fibrils, it leads to astonishingly large values for the tip indentation $\tilde{z}_0$ (Figure 10, dashed lines). In particular, a tip indentation of 5 nm into the collagen lawn is not consistent with its thickness of only 2−3 nm. This thickness was determined in a separate experiment from the plasma etching rate of collagen.[39] The reason for the large tip indentation values $\tilde{z}_0$ can be found in strong attractive interactions between the tip and sample, resulting in a width w of the attractive regime of about 4 nm.[49]

An alternative definition of the unperturbed sample surface is z_B, the position where a balance of attractive and repulsive forces is observed in the phase−distance curves. At this point, the transition from the attractive to the repulsive regime of tip−sample interaction occurs. For collagen fibrils, z_B is a better approximation of the unperturbed sample surface, and the resulting tip indentation $\tilde{z}_B$ is consistent with the thickness of the collagen lawn (Figure 10). For $\tilde{z}_B$, the relative differences in tip indentation between the gap and the overlap regions are the same as those for $\tilde{z}_0$.

Conflict of Interest: The authors declare no competing financial interest.

Acknowledgment. We thank A. Taubenberger and D.J. Müller for sharing details of their collagen sample preparation procedure, N. Drechsel for her contributions during the initial stage of the project, A. Süsselbeck for the sample preparation, C. Riesch for help with the data analysis, M. Dehnert, D. Voigt, and M. Uhlig for discussions, and S. McGee for proofreading the manuscript. Funding by the Volkswagen Foundation, the Deutsche Forschungsgemeinschaft, and the Gesellschaft für Arthroskopie und Gelenkchirurgie (AGA) is acknowledged.

REFERENCES AND NOTES

1. Fratzl, P., Ed. *Collagen: Structure and Mechanics*; Springer: Heidelberg, Germany, 2008.
2. Graßmann, W. Untersuchungen über Kollagen. *Kolloid Z.* **1936**, *77*, 205–209.
3. Baselt, D. R.; Revel, J. P.; Baldeschwieler, J. D. Subfibrillar Structure of Type I Collagen Observed by Atomic Force Microscopy. *Biophys. J.* **1993**, *65*, 2644–2655.
4. Stolz, M.; Raiteri, R.; Daniels, A.; VanLandingham, M. R.; Baschong, W.; Aebi, U. Dynamic Elastic Modulus of Porcine Articular Cartilage Determined at Two Different Levels of Tissue Organization by Indentation-Type Atomic Force Microscopy. *Biophys. J.* **2004**, *86*, 3269–3283.
5. Wenger, M. P. E.; Bozec, L.; Horton, M. A.; Mesquida, P. Mechanical Properties of Collagen Fibrils. *Biophys. J.* **2007**, *93*, 1255–1263.
6. Stolz, M.; Gottardi, R.; Raiteri, R.; Miot, S.; Martin, I.; Imer, R.; Staufer, U.; Raducanu, A.; Düggelin, M.; Baschong, W.; et al. Early Detection of Aging Cartilage and Osteoarthritis in Mice and Patient Samples Using Atomic Force Microscopy. *Nat. Nanotechnol.* **2009**, *4*, 186–192.
7. Yang, L.; van der Werf, D. M.; Fitié, C. F.; Bennink, M. L.; Dijkstra, P. J.; Feijen, J. Mechanical Properties of Native and Cross-Linked Type I Collagen Fibrils. *Biophys. J.* **2008**, *94*, 2204–2211.
8. Grant, C. A.; Brockwell, D. J.; Radford, S. E.; Thomson, N. H. Effects of Hydration on the Mechanical Response of Individual Collagen Fibrils. *Appl. Phys. Lett.* **2008**, *92*, 233902.

9. Grant, C. A.; Brockwell, D. J.; Radford, S. E.; Thomson, N. H. Tuning the Elastic Modulus of Hydrated Collagen Fibrils. *Biophys. J.* **2009**, *97*, 2985–2992.
10. Xia, D.; Zhang, S.; Hjortdal, J. O.; Li, Q.; Thomsen, K.; Chevallier, J.; Besenbacher, F.; Dong, M. Hydrated Human Corneal Stroma Revealed by Quantitative Dynamic Atomic Force Microscopy at Nanoscale. *ACS Nano* **2014**, *8*, 6873–6882.
11. Binnig, G.; Quate, C. F.; Gerber, C. Atomic Force Microscope. *Phys. Rev. Lett.* **1986**, *56*, 930–933.
12. Landis, W. J.; Silver, F. H.; Freeman, J. W. Collagen as a Scaffold for Biomimetic Mineralization of Vertebrate Tissues. *J. Mater. Chem.* **2006**, *16*, 1495–1503.
13. Nudelman, F.; Lausch, A. J.; Sommerdijk, N. A. J. M.; Sone, E. D. In Vitro Models of Collagen Biomineralization. *J. Struct. Biol.* **2013**, *183*, 258–269.
14. Gómez-Morales, J.; Iafisco, M.; Delgado-López, J. M.; Sarda, S.; Drouet, C. Progress on the Preparation of Nanocrystalline Apatites and Surface Characterization: Overview of Fundamental and Applied Aspects. *Prog. Cryst. Growth Charact.* **2013**, *59*, 1–46.
15. Kadler, K. E.; Holmes, D. F.; Trotter, J. A.; Chapman, J. A. Collagen Fibril Formation. *Biochem. J.* **1996**, *316*, 1–11.
16. Hassenkam, T.; Jørgensen, H. L.; Pedersen, M. B.; Kourakis, A. H.; Simonsen, L.; Lauritzen, J. B. Atomic Force Microscopy on Human Trabecular Bone from an Old Woman with Osteoporotic Fractures. *Micron* **2005**, *36*, 681–687.
17. Wallace, J. M.; Erickson, B.; Les, C. M.; Orr, B. G.; Banaszak Holl, M. B. Distribution of Type I Collagen Morphologies in Bone: Relation to Estrogen Depletion. *Bone* **2010**, *46*, 1349–1354.
18. Chernoff, E. A. G.; Chernoff, D. A. Atomic Force Microscope Images of Collagen Fibers. *J. Vac. Sci. Technol., A* **1992**, *10*, 596–599.
19. Raspanti, M.; Alessandrini, A.; Gobbi, P.; Ruggeri, A. Collagen Fibril Surface: TMAFM, FEG-SEM and Freeze-Etching Observations. *Microsc. Res. Tech.* **1996**, *35*, 87–93.
20. Heim, A. J.; Matthews, W. G.; Koob, T. J. Determination of the Elastic Modulus of Native Collagen Fibrils *via* Radial Indentation. *Appl. Phys. Lett.* **2006**, *89*, 181902.
21. Heim, A. J.; Koob, T. J.; Matthews, W. G. Low Strain Nanomechanics of Collagen Fibrils. *Biomacromolecules* **2007**, *8*, 3298–3301.
22. Grant, C. A.; Phillips, M. A.; Thomson, N. H. Dynamic Mechanical Analysis of Collagen Fibrils at the Nanoscale. *J. Mech. Behav. Biomed. Mater.* **2012**, *5*, 165–170.
23. Minary-Jolandan, M.; Yu, M.-F. Nanomechanical Heterogeneity in the Gap and Overlap Regions of Type I Collagen Fibrils with Implications for Bone Heterogeneity. *Biomacromolecules* **2009**, *10*, 2565–2570.
24. Paige, M. F.; Lin, A. C.; Goh, M. C. Real-Time Enzymatic Biodegradation of Collagen Fibrils Monitored by Atomic Force Microscopy. *Int. Biodeterior. Biodegrad.* **2002**, *50*, 1–10.
25. Hassenkam, T.; Fantner, G. E.; Cutroni, J. A.; Weaver, J. C.; Morse, D. E.; Hansma, P. K. High-Resolution AFM Imaging of Intact and Fractured Trabecular Bone. *Bone* **2004**, *35*, 4–10.
26. Lee, S. J.; Choi, S.; Kim, M. S.; Cheong, Y.; Kwak, H.-W.; Park, H. K.; Jin, K. H. Short-Term Effect of Cryotherapy on Human Scleral Tissue by Atomic Force Microscopy. *Scanning* **2013**, *35*, 302–307.
27. Spitzner, E.-C.; Riesch, C.; Szilluweit, R.; Tian, L.; Frauenrath, H.; Magerle, R. Multi-Set Point Intermittent Contact (MUSIC) Mode Atomic Force Microscopy of Oligothiophene Fibrils. *ACS Macro Lett.* **2012**, *1*, 380–383.
28. Bar, G.; Thomann, Y.; Brandsch, R.; Cantow, H.-J.; Whangbo, M.-H. Factors Affecting the Height and Phase Images in Tapping Mode Atomic Force Microscopy. Study of Phase-Separated Polymer Blends of Poly(ethene-*co*-styrene) and Poly(2,6-dimethyl-1,4-phenylene oxide). *Langmuir* **1997**, *13*, 3807–3812.
29. Bar, G.; Ganter, M.; Brandsch, R.; Delineau, L.; Whangbo, M.-H. Examination of Butadiene/Styrene-*co*-Butadiene Rubber Blends by Tapping Mode Atomic Force Microscopy. Importance of the Indentation Depth and Reduced Tip−Sample Energy Dissipation in Tapping Mode Atomic Force Microscopy Study of Elastomers. *Langmuir* **2000**, *16*, 5702–5711.
30. Knoll, A.; Magerle, R.; Krausch, G. Tapping Mode Atomic Force Microscopy on Polymers: Where Is the True Sample Surface? *Macromolecules* **2001**, *34*, 4159–4165.
31. Höper, R.; Gesang, T.; Possart, W.; Hennemann, O.-D.; Boseck, S. Imaging Elastic Sample Properties with an Atomic Force Microscope Operating in the Tapping Mode. *Ultramicroscopy* **1995**, *60*, 17–24.
32. Cleveland, J.; Anczykowski, B.; Schmid, A. E.; Elings, V. Energy Dissipation in Tapping-Mode Atomic Force Microscopy. *Appl. Phys. Lett.* **1998**, *72*, 2613–2615.
33. García, R.; Gómez, C. J.; Martinez, N. F.; Patil, S.; Dietz, C.; Magerle, R. Identification of Nanoscale Dissipation Processes by Dynamic Atomic Force Microscopy. *Phys. Rev. Lett.* **2006**, *97*, 016103.
34. Schröter, K.; Petzold, A.; Henze, T.; Thurn-Albrecht, T. Quantitative Analysis of Scanning Force Microscopy Data Using Harmonic Models. *Macromolecules* **2009**, *42*, 1114–1124.
35. Streeter, I.; de Leeuw, N. H. A Molecular Dynamics Study of the Interprotein Interactions in Collagen Fibrils. *Soft Matter* **2011**, *7*, 3373–3382.
36. Bell, E.; Ivarsson, B.; Merrill, C. Production of a Tissue-like Structure by Contraction of Collagen Lattices by Human Fibroblasts of Different Proliferative Potential *in Vitro*. *Proc. Natl. Acad. Sci. U.S.A.* **1979**, *76*, 1274–1278.
37. Elliott, J. T.; Tona, A.; Woodward, J. T.; Jones, P. L.; Plant, A. L. Thin Films of Collagen Affect Smooth Muscle Cell Morphology. *Langmuir* **2003**, *19*, 1506–1514.
38. Gurdak, E.; Roushet, P. G.; Dupont-Gillain, C. C. Factors and Mechanisms Determining the Formation of Fibrillar Collagen Structures in Absorbed Phases. *Colloid Surf., B* **2006**, *52*, 76–88.
39. Röper, S. Strukturuntersuchungen an biologischen Materialien mit Hilfe rasterkraftmikroskopiebasierender Nanotomographie. Ph.D. Thesis, Technische Universität Chemnitz, Germany, 2011; http://nbn-resolving.de/urn:nbn:de:bsz:ch1-qucosa-68803 (accessed May 5, 2015).
40. Wess, T. J.; Orgel, J. P. Changes in Collagen Structure: Drying, Dehydrothermal Treatment and Relation to Long Term Deterioration. *Thermochim. Acta* **2000**, *365*, 119–128.
41. Lees, S. Water Content in Type I Collagen Tissues Calculated from the Generalized Packing Model. *Int. J. Biol. Macromol.* **1986**, *8*, 66–72.
42. Spitzner, E.-C.; Riesch, C.; Magerle, R. Subsurface Imaging of Soft Polymeric Materials with Nanoscale Resolution. *ACS Nano* **2011**, *5*, 315–320.
43. Dietz, C.; Zerson, M.; Riesch, C.; Franke, M.; Magerle, R. Surface Properties of Elastomeric Polypropylenes Studied with Atomic Force Microscopy. *Macromolecules* **2008**, *41*, 9259–9266.
44. Mark, J. E., Ed. *Polymer Data Handbook*; Oxford University Press: New York, 2009.
45. Beaglehole, D.; Christenson, H. K. Vapor Adsorption on Mica and Silicon: Entropy Effects, Layering, and Surface Forces. *J. Phys. Chem.* **1992**, *96*, 3395–3403.
46. Asay, D. B.; Kim, S. H. Evolution of the Adsorbed Water Layer Structure on Silicon Oxide at Room Temperature. *J. Phys. Chem. B* **2005**, *109*, 16760–16763.
47. Asay, D. B.; Kim, S. H. Effects of Adsorbed Water Layer Structure on Adhesion Force of Silicon Oxide Nanoasperity Contact in Humid Ambient. *J. Chem. Phys.* **2006**, *124*, 174712.
48. Zitzler, L.; Herminghaus, S.; Mugele, F. Capillary Forces in Tapping Mode Atomic Force Microscopy. *Phys. Rev. B* **2002**, *66*, 155436.
49. García, R.; Pérez, R. Dynamic Atomic Force Microscopy Methods. *Surf. Sci. Rep.* **2002**, *47*, 197–301.
50. Sherman, R.; Hirt, D.; Vane, R. Surface Cleaning with the Carbon Dioxide Snow Jet. *J. Vac. Sci. Technol., A* **1994**, *12*, 1876–1881.
51. Asylum Research, Humidity Sensing Cell Accessory for the MFP-3D AFM. Santa Barbara, CA, USA; http://www.asylumresearch.com/Products/HumiditySensingCell/HumidityCellDSHR.pdf (accessed December 2, 2011).

52. Zhong, Q.; Inniss, D.; Kjoller, K.; Elings, V. Fractured Polymer/Silica Fiber Surface Studied by Tapping Mode Atomic Force Microscopy. *Surf. Sci.* **1993**, *290*, L688–L692.
53. Sader, J. E.; Chon, J. W. M.; Mulvaney, P. Calibration of Rectangular Atomic Force Microscope Cantilevers. *Rev. Sci. Instrum.* **1999**, *70*, 3967–3969.
54. Rasband, W. S. *Image J*; U.S. National Institutes of Health: Bethesda, MD, 1997−2014; http://imagej.nih.gov/ij/.